1994ApJ...421..101D

THE ASTROPHYSICAL JOURNAL, 421:101–114, 1994 January 20
© 1994. The American Astronomical Society. All rights reserved. Printed in U.S.A.

A NEAR-INFRARED SPECTROSCOPIC STUDY OF THE LUMINOUS MERGER NGC 3256. I. CONSTRAINTS ON THE INITIAL MASS FUNCTION OF THE STARBURST

RENÉ DOYON
Département de Physique, Université de Montréal and Observatoire du Mont Megantic C.P. 6128, Succ. A., Montréal (Qc), Canada H3C 3J7
R. D. JOSEPH
University of Hawaii, Institute for Astronomy, 2680 Woodlawn Drive, Honolulu, HI 96822
AND
G. S. WRIGHT
Joint Astronomy Center, 665 Komohana Street, Hilo, HI 96720
Received 1993 February 22; accepted 1993 July 20

ABSTRACT

Near-infrared spectroscopy of the central regions of the merger galaxy NGC 3256 is presented. The central 3″ of the nucleus show strong recombination lines of hydrogen, helium, and a prominent CO band absorption at 2.3 μm. These features suggest there is a large population of OB stars and red supergiants associated with a vigorous episode of star formation activity. The relative strength of several recombination lines and the slope of the 2.2 μm continuum indicate that the nucleus of NGC 3256 is affected by an extinction $A_k = 0.6$ mag.

A stellar population model is used for interpreting the observational properties of the galaxy. We show that the Brγ equivalent width and the strength of the CO band at 2.3 μm provide a simple tool for determining the age of a starburst event. A χ^2 analysis is presented which allows both the age of the burst and the slope of the initial mass function to be determined in a unique way. The analysis shows that the starburst started between 12 and 27 Myr ago. Given the dynamical mass observed in the nucleus of NGC 3256, our analysis yields an IMF index $[\psi(m) \propto m^{-\alpha}]\alpha < 2.2$ which is shallower than recently derived IMFs in the solar neighborhood and the Magellanic Clouds.

Subject headings: galaxies: individual (NGC 3256) — galaxies: interactions — galaxies: ISM — galaxies: starburst — infrared: galaxies

1. INTRODUCTION

NGC 3256 is a spectacular example of a merging galaxy. Its optical image shows knotty structures, with two tidal tails (see Schweizer 1986) indicative that this system was formed by the collision of two galaxies of approximately equal mass (Toomre & Toomre 1972). A kinematic study of the ionized gas has revealed the presence of noncircular motions (Feast & Robertson 1978), probably reminiscent of its violent past history. At a distance of 37 Mpc ($H_0 = 75$ km s^{-1} Mpc^{-1}), NGC 3256 has a total luminosity (8–1000 μm) of $3 \times 10^{11}\ L_\odot$ (Sargent, Sanders, & Phillips 1989) which makes this merger the most luminous galaxy at redshifts less than 3000 km s^{-1}. This galaxy is a powerful 10 μm source (Graham et al. 1984, 1987; Joseph & Wright 1985), and this emission is very extended; half of it originates outside the central kpc. This feature was interpreted by Graham et al. and Wright et al. (1988) as strong evidence that its extreme luminosity is powered by a recent episode of vigorous star formation activity. Sargent et al. (1989) have mapped the $J = 2 \rightarrow 1$ CO emission and derived a molecular mass of $3 \times 10^{10}\ M_\odot$ which is among the highest ever found in a galaxy. However, unlike other ultraluminous merging galaxies such as NGC 6240 and Arp 220, the molecular gas in NGC 3256 is very extended.

This wealth of observations and the relative proximity of NGC 3256 make this galaxy a very good candidate for studying starburst activity associated with merging galaxies. In this paper we present new near-infrared (IR) spectroscopic observations of NGC 3256. We present a new method for constraining the age of the burst and the parameters of the initial mass function (IMF). A second paper (Doyon, Wright, & Joseph 1994) focuses on the excitation mechanism of the conspicuous molecular hydrogen emission (H_2) observed in this galaxy. The main sections of the paper are divided as follows: the observations are described in § 2 and the main results outlined in § 3. Modeling of the observational properties of the galaxy is described in § 4. The main conclusions of this study are summarized in § 5.

2. OBSERVATIONS AND DATA REDUCTION

Near-infrared spectra of the nuclear regions of NGC 3256 were obtained at the Anglo-Australian Telescope on the nights of 1989 February 24–25, using the IR grating spectrometer FIGS (Bailey et al. 1988). The first position observed was centered on one of the brightest optical knots seen in the galaxy (position "T" in the notation of Feast & Robertson 1978) using a square aperture of 3.″5 × 3.″5. Previous IR aperture photometry of NGC 3256 (Joseph & Wright 1994) has shown that this position is, within a few arcseconds, coincident with the 2.2 μm peak. Based on the relative positions of nearby stars seen in Figure 1 and the coordinates given in the *HST Guide Star Catalogue*, we estimate the position of the 2.2 μm peak at $\alpha = 10^h25^m42^s.9$, $\delta = -43°38'54''$ (epoch 1950). Throughout the rest of the paper, we shall refer to this position as the 2.2 μm nucleus.

Full window spectra were obtained at J (1.11–1.32 μm), H (1.50–1.80 μm), and K (2.01–2.44) for the nucleus. Two other positions, 5″ east and 5″ south of the nucleus, were also observed at K using the same aperture. The three positions observed are shown overlayed on the optical image of the galaxy in Figure 1. This picture was reproduced from the pho-

© American Astronomical Society • Provided by the NASA Astrophysics Data System

1994ApJ...421..101D

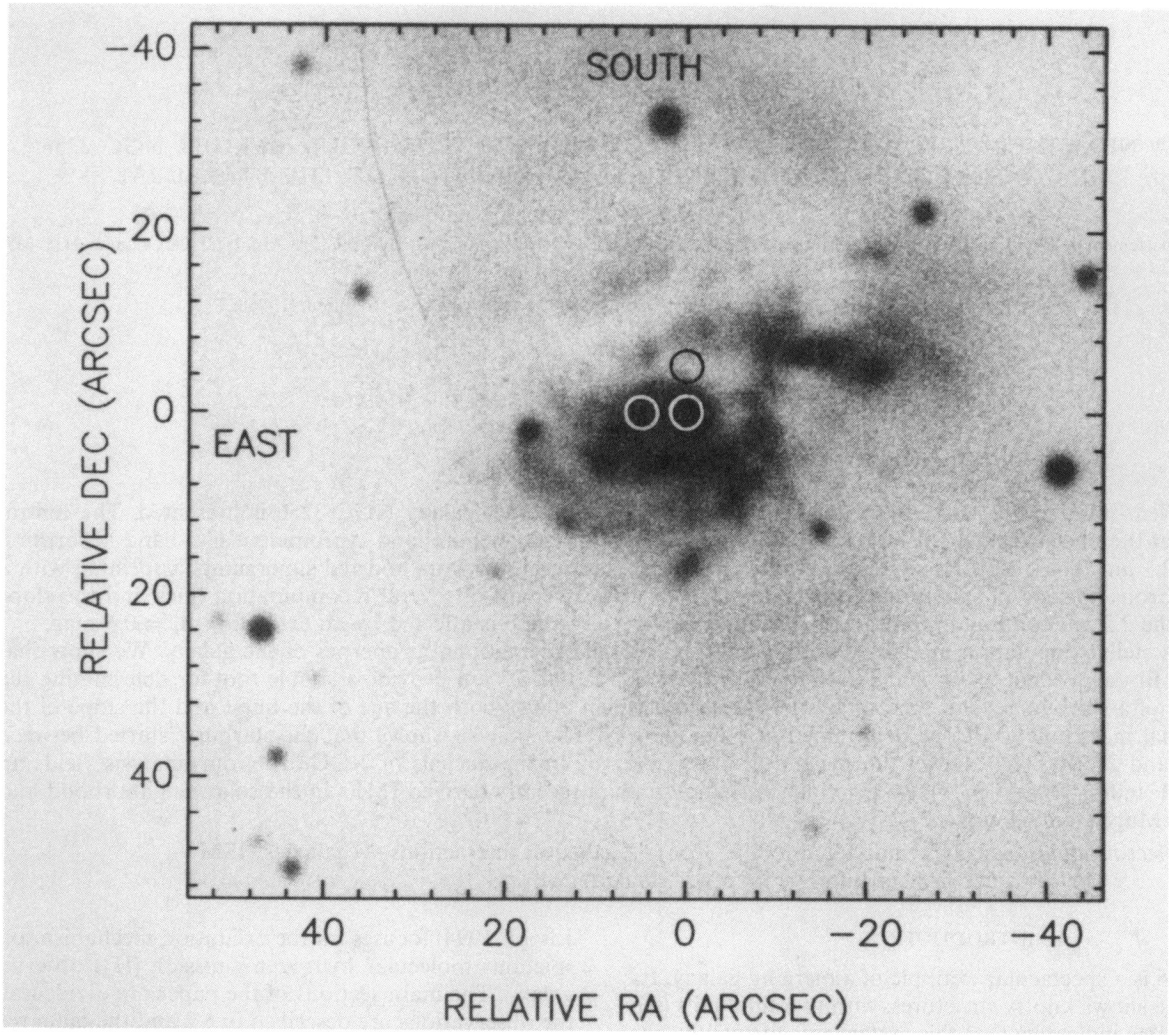

FIG. 1.—Optical photograph of the central region of NGC 3256 taken by D. S. Evans (see Feast & Robertson 1978, Fig. 1) and kindly provided by M. W. Feast. The three positions observed are shown as circles with diameters of the same size (3".5) as the side of the square aperture used. The position of the 2.2 μm nucleus defines the origin of the relative coordinates.

tograph of Feast & Robertson (1978) and kindly provided by M. W. Feast.

The instrument was set to a resolving power of 500 at K. The spectra were oversampled by scanning the 16 detectors of the grating over 13 steps, yielding 96 resolution elements in 208 channels. However, because the resolution of FIGS has a strong dependence on aperture size when the source is extended, a lower resolving power was achieved on the galaxy. Using the width of Brγ observed in NGC 3256 (see Fig. 2*a*), we derived a resolving power ($\lambda/\Delta\lambda$) of 280 assuming that the line is unresolved which is a very good assumption since Moorwood & Oliva (1988) marginally resolved Brγ in NGC 3256 with an intrinsic width of 300–400 km s^{-1} (only $\sim$7% of the line width at a resolving power of 280). The degradation of the resolving power from 500 to 280 meant that the galaxy spectra were effectively oversampled by a factor of $\sim$4 instead of 2 as initially intended. Similarly, using the width of Paβ (1.2822 μm) and [Fe II] 1.644 μm observed in the galaxy, we derived a resolving power of 370 and 400 (both $\pm$50) at J and H, respectively. Standard chopping and nodding techniques were employed; the chop throw was set to an amplitude of 60″ in the north-south direction.

The wavelength calibration system of the instrument was unavailable at the time of the observations, and the spectra had to be calibrated with atmospheric absorption and emission lines. Water and CO_2 absorption features at 2.0602 and 1.1346 μm were used for the K and J spectra, respectively. The calibration at H was achieved using OH emission bands observed on the sky. The accuracy of this calibration was found to be better than half a resolution element which was good enough to correct the wavelength shift (typically a few resolution elements) caused by the systematic drift of the grating, observed after moving the telescope to a new position.

The atmospheric transmission and the relative sensitivity of the detectors were corrected by dividing all the spectra with the spectrum of the standard star BS 4013 (G1V) observed at an air mass similar ($<$0.05) to the galaxy. The flux calibration was achieved with the same star assuming a K-magnitude of 5.01 and an energy distribution as given in the software package FIGARO (see Allen 1989). Intrinsic K-window absorption lines in the standard were removed by dividing the star with the high-resolution rectified spectrum of 16 Cyg A (G3V) taken from the stellar atlas of Kleinmann & Hall (1986) after convolution with a Gaussian instrumental profile with $\lambda/\Delta\lambda = 280$.

© American Astronomical Society • Provided by the NASA Astrophysics Data System

1994ApJ...421..101D

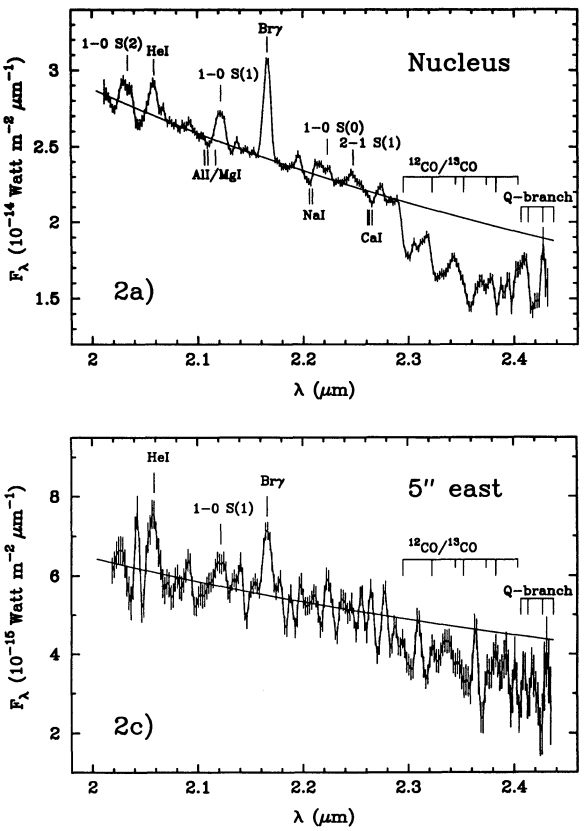

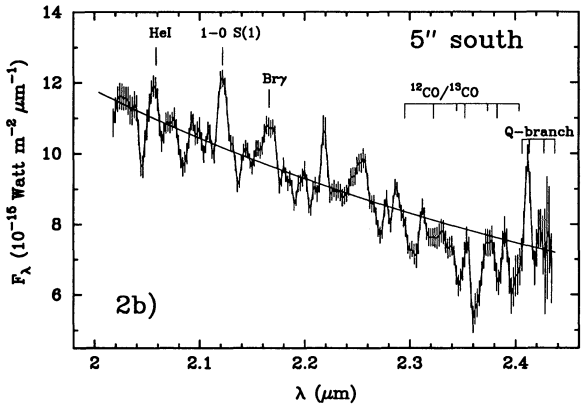

FIG. 2.—*K*-window spectra of NGC 3256: (*a*) nucleus, (*b*) 5″ south, and (*c*) 5″ east of the nucleus. The spectra are shown in the rest frame of the galaxy. Each spectral point is plotted with an error bar of $\pm 1\ \sigma$. The solid lines are the best fit to a power-law spectrum ($F_\lambda \propto \lambda^\beta$) fitted from featureless sections of the continuum taken between 2.0 and 2.29 μm. Except for (*a*), all spectra have been smoothed with a three-point triangular filter. Note however that the fluxes given in Table 1 have been derived from unsmoothed spectra.

This correction has virtually no effect on the shape of the galaxy spectrum except for the removal of a spurious emission feature due to Brγ absorption in the standard star. Such correction was not applied for the *J*- and *H*-window spectra because of the lack of a template spectrum in these bands. The uncertainty of the absolute calibration is ~10% as estimated from the scatter of the mean of several spectra obtained during both nights.

3. RESULTS

3.1. *Emission Lines*

All the spectra obtained at *K* are shown in Figures 2*a*–2*c*. These were obtained after an integration of 3 hours for the nucleus and 1 hour for the other two positions. The quality of the spectrum obtained on the nucleus is very good. The average signal-to-noise ratio per point measured for the whole spectrum is ~80 and more than 100 between 2.0 and 2.3 μm. The spectra are shown in their rest frame. This was done by shifting and scaling the spectra such that either Brγ (2.1661 μm) or the 1–0 *S*(1) (2.1218 μm)—whichever strongest in a given spectrum—are centered at their respective rest wavelength in the vacuum.

As shown in Figure 2*a*, the nucleus spectrum show several emission features, but we do not necessarily regard all of them as genuine emission lines since many of these coincide with known OH transitions emitted from the sky. These spurious features could have appeared in our spectra as residuals due to an imperfect atmospheric cancellation. This is probably the case of the emission features found (in the rest frame of the galaxy) at 2.03, 2.092, 2.196, and 2.215 μm (see Fig. 2*a*). Even though we cannot exclude that these emission features are real, we adopt the conservative approach of considering only detection (3–4 σ) of emission lines which are at least a resolution element (4 pixels) away from any OH transitions.

Integrated line fluxes and their corresponding wavelengths as measured from the spectra are listed in Table 1. The intensities of strong emission lines were measured by adding all the flux relative to the local continuum and by fitting Gaussian profiles (with a FWHM constrained by the strong lines) for faint lines and blended features. The errors on the flux given in Table 1 are *statistical* only and do not include a contribution from the uncertainties in the continuum fit and the absolute calibration.

The dominant emission lines observed in the *K* spectra are Brγ, the singlet $2^1\ S$–$2^1\ P^o$ transition of He I (2.0587 μm), and the 1–0 *S*(1) of H_2, the latter being marginally detected in the 5″ east spectrum. The observed line fluxes on the nucleus for the 1–0 *S*(1) and Brγ are $1.8 \pm 0.1 \times 10^{-17}$ and $5.4 \pm 0.1 \times 10^{-17}$ W m^{-2}, respectively. Adding the flux detected at the other positions off the nucleus gives line fluxes which are higher (especially for Brγ) by 25%–30% compared with the 6″ × 6″ aperture measurements of Moorwood & Oliva (1988). This discrepancy is probably not significant given the uncertainties in comparing different aperture measurements and possible errors in the relative pointing and absolute calibration of two set of observations.

The relative strengths of the emission lines on the nucleus and the southern position strongly suggest that the H_2 is much more extended than the Brγ emission. Indeed, while the 1–0 *S*(1) flux remains nearly constant going from the nuclear to the southern position, Brγ decreases by a factor of 3.5. That the H_2 is relatively more extended than Brγ is a result that has been previously noted in other mergers based on multi-aperture spectroscopic measurements (Joseph et al. 1987; Prestwich 1989). Other transitions of H_2 were also detected on the nucleus. These include the 1–0 *S*(2) (2.0338 μm), 1–0 *S*(0) (2.2233 μm), 2–1 *S*(1) (2.2477 μm), and the first three transitions of the 1–0 Q-branch. A full discussion on the excitation mechanism of the H_2 emission observed in NGC 3256 is presented in Doyon et al. (1994).

The spectra of the nucleus obtained in the *J* and *H* bands are shown in Figures 3*a* and 3*b*, respectively. We identify the

© American Astronomical Society • Provided by the NASA Astrophysics Data System

1994ApJ...421..101D

TABLE 1

LINE FLUXES AND IDENTIFICATIONS IN NGC 3256

OBSERVED WAVELENGTH (μm)	INTEGRATED FLUX (10^{-17} W m^{-2}) Observed	Dereddened	IDENTIFICATION
		Nucleus	
1.255(1).....	3.3 ± 1	12.9	He I 3^3S–4^3P^o 1.2531
1.259(1).....	3.2 ± 1	12.3	[Fe II] a^6D_1–a^4d_7 1.2573
1.282	14.2 ± 1	52.3	Paβ 1.2822
1.644	4.5 ± 0.1	10.4	[Fe II] a^4D_1 1.644
2.036(3).....	0.8 ± 0.3	1.4	H_2 1–0 $S(2)$ 2.0338
2.058(<1)	1.8 ± 0.2	3.2	He I 2^1S–2^1P^o 2.0587
2.122(<1)	1.8 ± 0.1	3.1	H_2 1–0 $S(1)$ 2.1218
2.166	5.4 ± 0.1	9.1	Brγ 2.1661
2.224(1).....	0.5 ± 0.1	0.8	H_2 1–0 $S(0)$ 2.2233
2.247(1).....	0.7 ± 0.1	1.2	H_2 2–1 $S(1)$ 2.2477
2.427(<1)	1.6 ± 0.5	2.5	H_2 1–0 $Q(3)$ 2.4237
		5″ South	
2.057(2).....	0.9 ± 0.3	...	He I 2^1S–2^1P^o 2.0587
2.122	2.1 ± 0.2	...	H_2 1–0 $S(1)$ 2.1218
2.167(1).....	1.5 ± 0.2	...	Brγ 2.1661
2.247(3).....	0.6 ± 0.3	...	H_2 2–1 $S(1)$ 2.2477
		5″ East	
2.057(1).....	1.4 ± 0.3	...	He I 2^1S–2^1P^o 2.0587
2.122(2).....	0.7 ± 0.2	...	H_2 1–0 $S(1)$ 2.1218
2.166	1.7 ± 0.2	...	Brγ 2.1661
2.223(2).....	0.6 ± 0.2	...	H_2 1–0 $S(0)$ 2.2233

[a] Rest-frame wavelengths as measured from the spectra relative to the following lines (assumed to be correctly identified): Paβ and Brγ for the nucleus, 1–0 $S(1)$ for the southern spectrum, and Brγ for the eastern spectrum. The number in parentheses gives the error in units of 0.001 μm. No error is given for reference lines.

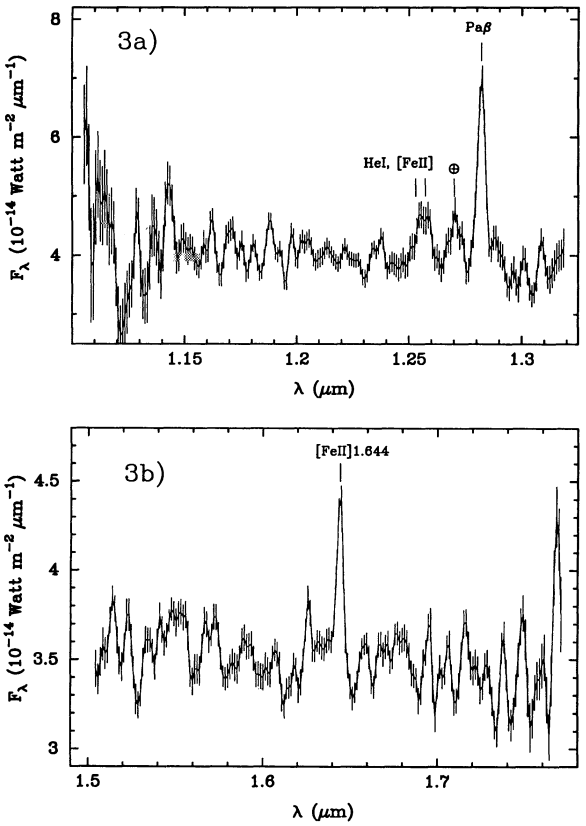

FIG. 3.—J and H spectra of NGC 3256 obtained on the nucleus. As in Fig. 2, the spectra are shown in the rest frame. The emission feature marked by the symbol "⊕" in the J spectrum is probably spurious and due to Paβ absorption in the standard star, used to ratio the raw galaxy spectrum.

strongest emission line in the J spectrum with Paβ (1.2822 μm). The emission feature at $\approx$1.26 μm is probably a blend of the two transitions of He I (1.253 μm) and [Fe II] (1.257 μm). Fluxes for these lines are given in Table 1. The emission line around 1.27 μm is coincident with the expected position of Paβ blueshifted by the systemic velocity of NGC 3256. We thus associate this line with Paβ absorption in the standard star which appears in our spectrum as a spurious emission line after ratioing the galaxy spectrum with that of the standard.

We identify the strong emission line in the middle of the H spectrum with the transition of [Fe II] at 1.644 μm. This line is also very close to a transition of [Si I] at 1.6459 μm, and although our wavelength scale is not accurate enough to exclude that possibility, we dismiss this identification on the basis that we also detected a transition of [Fe II] in the J-window (see above). Furthermore, if the line at 1.644 μm is [Si I] then we would expect to detect another [Si I] line at 1.067 μm which should be a factor of 3 weaker than the 1.6459 μm transition (Graham, Wright, & Longmore 1987). Such a strong line should have been detected in our spectrum, given the signal-to-noise of the 1.644 μm line, but this is clearly not the case (see Fig. 3*b*).

3.2. *Absorption Lines*

The spectrum of the nucleus also shows a number of absorption lines. As previously noted for emission lines, a bad cancellation of atmospheric OH lines could potentially produce spurious absorption features, especially shortward of 2.25 μm where the OH lines are mostly observed. We note also that the absorption features observed at $\sim$2.04 and $\sim$2.06 μm (after redshifting the spectrum) in Figure 2*a* are probably spurious and due to an imperfect cancellation of the strong atmospheric absorption feature of CO_2 at 2.054 and 2.065 μm.

The strongest absorption feature in the K spectrum is the CO band longward of 2.29 μm. The strength of the CO band was quantified by a *spectroscopic* CO index defined as follows:

$$CO_{sp} = -2.5 \log \langle R_{2.36} \rangle \quad (1)$$

where $\langle R_{2.36} \rangle$ is the average of the rectified spectrum R_λ between 2.31 and 2.40 μm in the rest frame of the galaxy. The rectified spectrum is obtained by ratioing the observed spectrum with a power-law continuum fitted from featureless sections of the spectrum. More details about this spectroscopic approach for measuring the depth of the CO band are given in Appendix A along with spectroscopic CO indices of all the stars observed by Kleinmann & Hall (1986). Spectroscopic CO indices and power-law indices for all positions are given in Table 2. Note that the errors given for CO_{sp} include the uncertainties in placing the continuum level.

Absorption features due to transitions of Na I ($\sim$2.206 μm) and Ca I ($\sim$2.263 μm) are also identified in the nuclear spectrum. As given in Table 2, the Na I and Ca I absorption features have an average equivalent width of 1.9 ± 0.4 Å, but this value increases to 2.9 ± 0.4 Å after correction for a 10% contribution of featureless continuum (see § 4.1). This latter value is similar to the average equivalent width measured in a K5III star spectrum, which represents to a very good approximation the energy distribution of normal galaxies (Frogel et al. 1978;

© American Astronomical Society • Provided by the NASA Astrophysics Data System

1994ApJ...421..101D

TABLE 2

CONTINUUM SLOPES AND ABSORPTION LINE STRENGTHS

Spectrum	β[a]	Na I (Å)	Ca I (Å)	CO_{sp}
Nucleus	-2.16 ± 0.04	1.9 ± 0.4	1.8 ± 0.5	0.23 ± 0.01
5″ south	-2.49 ± 0.09	...	...	0.11 ± 0.02
5″ east	-2.00 ± 0.17	...	...	0.24 ± 0.03
γ Dra (K5III)	-3.58	3.3	2.9	0.20

[a] Power-law index ($F_\lambda \propto \lambda^\beta$) fitted to the continuum between 2.0 and 2.3 μm.

Arnaud & Gilmore 1986; Frogel 1985). Thus, the strength of both Na I and Ca I absorption features are consistent with that expected for normal galaxies. Finally, we suggest that the local depression of the continuum near 2.1 μm is due to absorption lines of Al I and Mg I.

These absorption lines are common features in spectra of late-type stars (see Kleinmann & Hall 1986) and provide strong evidence that *most of the* 2.2 μm *continuum observed in NGC 3256 has a stellar origin.*

3.3. *Extinction*

Our spectra provide three independent methods for determining the extinction toward the nucleus of the galaxy. The most accurate one is probably provided by the ratio of Paβ to Brγ. Assuming the validity of case B for the observed recombination spectrum, the intrinsic Paβ/Brγ line ratio is expected to be 5.89 for $T_e = 10^4$ K and $n_e = 10^4$ cm^{-3} (Hummer & Storey 1987). We observed a ratio of 2.7 ± 0.3 on the nucleus corresponding to a relative extinction of 0.89 mag. Assuming an extinction law that varies as $\lambda^{-1.75}$ (Draine 1989), this corresponds to an absolute extinction at 2.2 μm of 0.55 ± 0.09 mag, that is, $A_V = 5.5$. We can also use the ratio of [Fe II] 1.257 to [Fe II] 1.644. The extinction derived from these lines has the major advantage of being independent of temperature since the two transitions arise from the same upper level. From the Einstein coefficients of Nussbaumer & Storey (1988), we derive an intrinsic [Fe II] 1.257/[Fe II] 1.644 line ratio of 1.36. The line fluxes given in Table 1 imply $A_K = 0.7 \pm 0.3$.

Finally, the extinction can be derived from the slope of the continuum in the K spectrum. One has to make the assumption that the integrated light of the galaxy is well approximated by K5III stars, which is a good approximation as pointed out earlier. We have compared the slope of the galaxy spectrum with that of a K5III star, taken from the Kleinmann & Hall (1986) atlas, by fitting a power-law index ($F_\lambda \propto \lambda^\beta$) to the continuum between 2.0 and 2.3 μm. The power-law indices listed in Table 2 clearly show that the nucleus has a flatter continuum than the K5III star, suggesting that the 2.2 μm continuum of the galaxy is affected by extinction. To make the galaxy continuum slope equal to that of the star requires an absolute extinction at 2.2 μm of 0.8 ± 0.1. This figure is certainly an upper limit since the continuum is most likely contaminated by warm dust, as discussed later in § 4.1. Correcting the spectrum with 4% contribution (see § 4.1) of a gray body spectrum yields $A_K = 0.6$.

It thus seems that within the errors, the extinction derived from the ionized gas and the stars is the same in NGC 3256. A similar result was found by Lester et al. (1990) in M82. It is important to note that our reddening estimates were derived under the assumption that the stars and the ionized gas are affected by *foreground* extinction only, that there is no dust between the emitting sources. If internal reddening is important, then the extinction derived under the assumption that it is foreground will be much lower. Whether internal reddening is important in NGC 3256 needs to be assessed with a measurement of Brα, and for the rest of the paper an extinction of $A_K = 0.55$ mag will be assumed, bearing in mind that this value could well be a lower limit if internal reddening is important.

4. MODELING THE LINE AND CONTINUUM EMISSION

As discussed in the Introduction, there is compelling evidence that the nuclear region of NGC 3256 is experiencing a burst of star formation. We show in the next section that our spectroscopic observations strengthen this interpretation. The observational properties of the galaxy will then be used along with an evolutionary starburst model to constrain both the age of the burst and the parameters of the IMF.

4.1. *Evidence for Starburst Activity in NGC 3256*

Since the K continuum of NGC 3256 is reminiscent of late-type stars (see § 3.2), it is natural to suppose that the activity observed in this galaxy is associated with an episode of vigorous star formation. In this context, the ionization observed in NGC 3256 is most likely associated with young OB stars. At a distance of 37 Mpc, the nuclear Brγ flux corresponds to a luminosity (corrected for extinction) of 3.8×10^6 $L_\odot$ or an ionization rate of 1.14×10^{54} s^{-1} for the central 600 pc, similar to the value inferred in the archetypal starburst M82 within the same physical region (Puxley et al. 1989). Such a high ionization rate can only be maintained by massive star formation.

As discussed in Doyon, Puxley, & Joseph (1992), the He I λ2.06 μm/Brγ line ratio can be used to determine the average spectral type of the hot stellar population. They showed that this ratio has a steep dependence on effective temperature. The ratio of 0.35 ± 0.04 observed on the nucleus implies an effective temperature of $\sim$35,000 K which corresponds to an O8 main-sequence star. Representing all the ionizing stars in the nucleus by this average spectral type, 6.9×10^5 such stars are required to explain the Brγ luminosity observed in the central 600 pc of NGC 3256. This population of young stars has a total mass of 1.5×10^7 $M_\odot$ and a bolometric luminosity of 9.2×10^{10} $L_\odot$. This is very close to 8.7×10^{10} $L_\odot$, derived from the small aperture 10 μm measurement of Graham et al. (1987), calculated using the extrapolation $L_{IR} = 15 L_{10\mu m}$ (Scoville et al. 1983; Telesco & Gatley 1984) after correction for an extinction 0.26 mag at 10 μm. This luminosity can account for a third of the total 3×10^{11} $L_\odot$ deduced from the *IRAS* and 10 μm data (Sargent et al. 1989; Graham et al. 1984, 1987).

The detection of Brγ outside the nucleus (see Figs. 2*b* and 2*c*) demonstrates that star formation is also active at these positions, but the level of this activity is uncertain because the extinction is not well determined for these regions. Inspection of Figure 1 suggests that the region 5″ south is probably affected by strong reddening as there is little optical emission at this position relative to the nucleus. The visual extinction at this position could well be as much as 5–10 mag higher than that on the nucleus, implying that most of the ionizing stars are still embedded in molecular clouds.

The strength of the 2.3 μm CO band in NGC 3256 provides further evidence for starburst activity. The spectroscopic CO index measured in the nucleus is 0.23 ± 0.01 (see Table 1) which is 3 σ stronger than observed in normal galaxies. Indeed, normal galaxies have typical *photometric* CO indices of 0.15

© American Astronomical Society • Provided by the NASA Astrophysics Data System

1994ApJ...421..101D

(Frogel et al. 1978), which after transformation (see Appendix A) corresponds to a CO_{sp} of 0.20. However, the spectroscopic CO index observed in NGC 3256 is only a lower limit estimate of the intrinsic CO band strength because of the possible contamination of the stellar K light by nonstellar sources such as hot dust and free-free emission. Since these sources have a featureless continuum, they will dilute the luminosity of late-type stars, hence reducing the depth of the CO band. This effect is not negligible in NGC 3256. The K continuum is contaminated by hot dust as suggested by the red $JHKL$ colors and strong $K-L$ excess (~ 1.0) observed within the central 15″ of the nucleus (Graham et al. 1987). Assuming a dust temperature of 500 K and an emissivity varying linearly with frequency, it can be estimated that 4%–5% of the 2.2 μm continuum is associated with hot dust. The free-free contribution can be calculated from the Brγ flux using the theoretical Brγ to free-free continuum ratio of Joy & Lester (1988). The Brγ flux given in Table 1 and the observed 2.2 μm flux density yield 4% for the contribution of free-free emission to the 2.2 μm continuum. Thus, an overall contribution of $\sim 10\%$ of the K luminosity is associated with featureless continuum. Correcting for this contribution gives a new spectroscopic CO index of 0.26 for the nucleus, which is now significantly stronger than expected for a normal stellar population.

This anomalously strong CO band implies the existence of a young population of red supergiants since these stars have stronger CO bands compared with giants of the same effective temperature (see Table 5 in Appendix A). As shown in the next section, the strength of the CO band associated with a young stellar population reaches a maximum between 15 and 40 Myr with a spectroscopic CO index of ~ 0.28. This increase of about 0.1 mag relative to normal galaxies is due to the sudden occurrence of red supergiants in the stellar population. Adopting the conservative assumption that the starburst is at a stage near its peak of strongest CO band, then the spectroscopic CO index of 0.26 observed in NGC 3256 implies that, *at least*, 75% of the 2.2 μm continuum is associated with a starburst population.

It is often argued that the interpretation of the CO band is complicated by the fact that its strength also depends on metallicity, the higher the metal abundance the stronger the depth of the CO band. This effect has been measured in globular clusters and a calibration between the *photometric CO index* and metallicity has been established by these observations (Frogel, Cohen, & Persson 1983). Using this calibration and the transformation between photometric and spectroscopic CO indices (see Appendix A) we have $\Delta CO_{sp} = 0.11\Delta[\mathrm{Fe/H}]$ where [Fe/H] is the logarithm of the metal abundance relative to the Sun. In this context, the strong CO band observed in NGC 3256 could be accounted for if the metal abundance in this galaxy is more than 3 times higher than the average metallicity of normal spirals which can reasonably be assumed to be solar.

However, there are two reasons to believe that a metallicity effect is not responsible for the strong CO band observed in NGC 3256. First, the calibration used to relate the CO band strength and metallicity has been determined from observations of globular clusters, most of them with metal abundances below solar. It is far from clear whether the extrapolation of this calibration is valid beyond solar metallicity. It should be remembered that the main reason why the CO band is stronger in supergiants compared with giants is because the former have a higher microturbulent velocity which is strong evidence that the CO absorption band is made of many saturated lines (McGregor 1987). Thus, if most of the CO lines are saturated, increasing the metallicity will have little effect on the strength of the molecular band.

Finally, if the stellar population in NGC 3256 is normal, except for its high metallicity, then its absolute K-magnitude should be comparable to other galaxies. On the nucleus, we measured an absolute K-magnitude (corrected for extinction) of -22.6 (see Table 3) which is 6 times brighter than the most luminous Sc spirals (Devereux, Becklin, & Scoville 1987). This means that less than 20% of the K continuum is contributed by an old population. Clearly, another source must be responsible for this high 2.2 μm luminosity, and the most plausible candidate is a population of young red supergiants.

One can estimate the number of red supergiants given the observed 2.2 μm luminosity and assuming that their progenitors are O8V stars (20 $M_\odot$) that will eventually become K4 supergiants after 10 Myr (Maeder & Meynet 1988) with an absolute K-magnitude of -10.8. Depending on whether a preexisting population is contributing at K, we estimate that $(3\text{–}5) \times 10^4$ red supergiants are required to account for the 2.2 μm luminosity in NGC 3256. Comparing with the number of O8V stars derived earlier, we have a O8V to red supergiant ratio between 14 and 23. These values are roughly consistent with the blue-to-red supergiant ratio of 10–40 observed in our own Galaxy (Humphreys 1978). Although such comparison is only approximate, the purpose of this simple analysis is to demonstrate that both the ionization state and 2.2 μm luminosity are consistent with the hypothesis that there are numerous OB stars and red supergiants present in the nucleus of NGC 3256.

In the following, we use an evolutionary model to put more quantitative constraints on the age of the burst and the parameters of the initial mass function.

4.2. *The Age of the Burst*

In order to constrain the age of the burst, observable quantities have to be related to a stellar population model. The results presented below were obtained with a stellar population model based on a set of evolutionary tracks (Maeder & Meynet 1988) with masses ranging from 0.85 to 120 $M_\odot$. Unlike previous models, these tracks include the effect of mass loss in the stellar evolution, which allows stars to come back to the left of the HR diagram after the red supergiant phase. The modeling procedure employed is very similar to the one described by Huchra (1977), a model used later by Rieke et al. (1980) in their study of the starburst galaxies M82 and NGC

TABLE 3

OBSERVATIONAL PROPERTIES OF THE NUCLEAR REGION OF NGC 3256[a]

	Nucleus	5″ South	5″ East
M_K^{tot}	-22.64 ± 0.05	-21.77 ± 0.05	-21.12 ± 0.05
$M_K^{corr\ b}$	-22.55 ± 0.05	-21.68 ± 0.05	-20.97 ± 0.05
$CO_{sp}^{corr\ b}$	0.26 ± 0.01	0.12 ± 0.02	0.27 ± 0.03
$\log N_{Lyc}(s^{-1})$	54.06 ± 0.04	53.50 ± 0.07	53.55 ± 0.05
$\log W_{Br\gamma}(\text{Å})^b$	1.40 ± 0.01	1.21 ± 0.05	1.52 ± 0.03
He I 2.06 μm/Brγ	0.35 ± 0.04	0.6 ± 0.2	0.8 ± 0.2
$\log N_{Lyc}/L_{IR}$	43.12 ± 0.08	...	...
$f_K^{HD\ c}$	>0.05	>0.05	>0.05
$f_K^{ff\ c}$	0.04	0.03	0.05

[a] All quantities have been corrected for extinction when appropriate.

[b] Corrected for free-free and hot dust emission.

[c] Fraction of the K continuum contributed by hot dust (f_K^{HD}) and free-free (f_K^{ff}) emission, calculated as described in the text.

© American Astronomical Society • Provided by the NASA Astrophysics Data System

1994ApJ...421..101D

253. A more detailed description of this model is presented in Appendix B.

The basic ingredients of the model are the following: the IMF, defined as the number of stars formed per unit mass interval, the star formation rate (SFR), and the age of the burst. The IMF is parameterized by a power law of the mass with an index $\alpha[\psi(m) \propto m^{-\alpha}]$ and a lower and an upper mass limit, m_l and m_u. For instance, the Salpeter (1955) IMF is characterized by $\alpha = 2.35$, whereas Scalo (1986) parameterizes the IMF with three power-law segments, the upper end having $\alpha \sim 2.85$. Three time dependences were investigated for the SFR: constant, exponential $[SFR \propto \exp(-t/\tau_0)]$, and "delayed" $[SFR \propto t \exp(-t/\tau_0)]$ where τ_0 is the timescale of the burst, arbitrarily set to 20 $Myr_\odot$. The model can predict the bolometric and 2.2 μm luminosity, ionization rates for photons with energy above 13.6 and 24.6 eV, spectroscopic CO index, and other quantities that will be discussed later. Note that the model does not incorporate the effect of an old preexisting population nor does it predict the contribution of nebular continuum from free-free and hot dust emission.

Ideally, one would like to constrain the model with quantities that are distance-independent and weakly dependent on extinction. We can define four NIR parameters that can satisfy the first requirement but not necessarily the second one. These are: the Brγ equivalent width, $W_{Br\gamma}$, defined as the ratio of the integrated Brγ flux to the local flux density F_λ, the spectroscopic CO index, CO_{sp}, the He I λ2.06 μm/Brγ ratio, and the ratio of the ionization rate to the bolometric luminosity, N_{Lyc}/L_{IR}, the ionization rate being derived from the Brγ flux. These quantities are given in Table 3 for the nuclear region of NGC 3256. The total luminosity, L_{IR}, was estimated from a 10 μm measurement made in a 3".5 aperture (see § 4.1) and corrected for extinction. Both $W_{Br\gamma}$ and CO_{sp} were corrected for the contribution of free-free and hot dust emission to the K continuum since these two types of emission were not treated in the model. The fraction of the K luminosity contributed by hot dust and free-free emission were estimated as described in § 4.1 and are given in Table 3 as f_K^{HD} and f_K^{ff}, respectively.

The time dependence of the four quantities described above is shown in Figure 4. This was calculated using a Salpeter IMF with lower and upper mass limits of 0.1 and 30 $M_\odot$, respectively. Although all these quantities could be used in principle for constraining the age, the spectroscopic CO index and the Brγ equivalent width are probably best suited for that purpose since they show a sharp variation on a short timescale. The strong time dependence of CO_{sp} and $W_{Br\gamma}$ is easy to understand. Before 8 Myr, the stellar population is dominated by young OB stars which produce strong ionization but little K continuum. This results in a large Brγ equivalent width and a negligible CO band. The near discontinuity in both CO_{sp} and $W_{Br\gamma}$ at 8–9 Myr is due to a sudden increase of the K luminosity associated with the first red supergiants appearing in the stellar population.

The spectroscopic CO index of 0.26 and the logarithmic Brγ equivalent width of 1.40 observed on the nucleus of NGC 3256 (see Table 3) imply a relatively narrow range for the age of the burst, between 10 and 25 Myr, depending on the detailed shape of the SFR (see Fig. 4). The observed and predicted values for the He I λ2.06 μm/Brγ ratio and log N_{Lyc}/L_{IR} are also consistent with this age interval. One should note that the age estimated from CO_{sp} and $W_{Br\gamma}$ remains between the range above even if we correct both quantities for a 20% continuum contribution from a preexisting old stellar population. It is worthwhile to note that the age of the burst inferred above is much smaller than the dynamical age of the merger. Indeed, the tidal tails observed in NGC 3256 are merger signatures that take 10^8–10^9 yr to develop (Schweizer 1986). It is not clear whether it takes that long to develop a starburst. If, instead, a starburst event occurs almost coincidently with the merger process, this would imply—although very speculative—that the current and very young starburst event observed in NGC 3256 is not the first one, that other similar events have occurred since the beginning of the merger process.

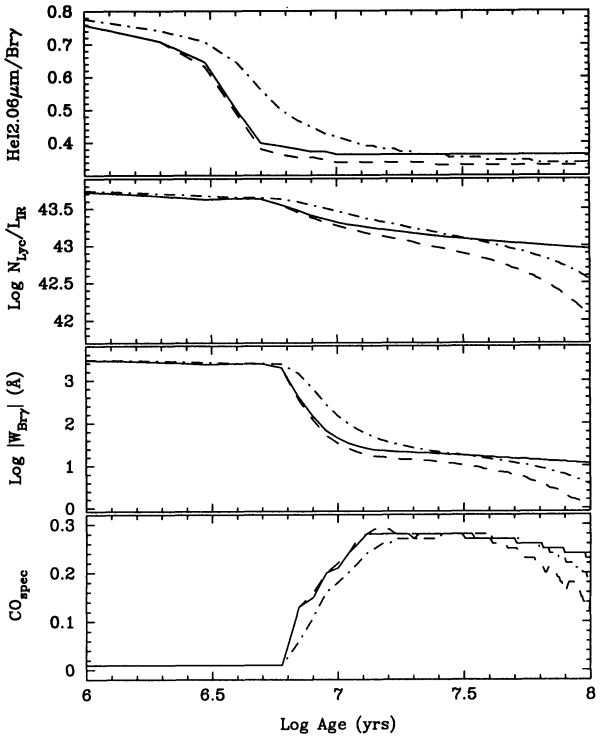

FIG. 4.—Continuum and emission line evolution of a young stellar population (the quantities are defined in the text), calculated with a population synthesis model, using a Salpeter IMF with $m_l = 0.1$ and $m_u = 30\ M_\odot$. The three lines of each plot correspond to different star formation rates: constant (*solid line*), exponential (*dashed line*), and "delayed" (*dashed-dotted line*).

Although an accurate determination of the age of a starburst system requires a detailed knowledge of the time dependence of the SFR, *the Brγ equivalent width and the spectroscopic CO index provide a simple tool for estimating the age of the burst.* In the following, we investigate how the four NIR quantities defined above can be used to further constrain the age, and also the parameters of the IMF.

4.3. *The Initial Mass Function*

Whether the IMF in starbursts is significantly different from that in the solar neighborhood is probably the most important question that has been raised by recent studies of these galaxies. Over the past few years, evidence has accumulated to suggest that galaxies with vigorous star formation activity are deficient in low-mass stars, a result usually referred as the lower mass limit being anomalously high or the IMF index significantly flatter than observed in the solar neighborhood (see Scalo 1989 for a review of the subject). There is already some evidence for a "top-heavy" IMF in NGC 3256. In their IR study of interacting galaxies, Wright et al. (1988) showed that the small mass-to-light ratio in NGC 3256 can be

© American Astronomical Society • Provided by the NASA Astrophysics Data System

1994ApJ...421..101D

accounted for only if the Miller-Scalo IMF (1979) is truncated at the lower end around 6 $M_\odot$. We shall show in this section that the near-IR spectroscopic properties of NGC 3256 are consistent, at least qualitatively, with that conclusion.

Basically, there are three parameters to constrain: the IMF index, α, and the lower and upper mass limits, m_l and m_u. The upper mass limit is probably the least constrained parameter, and values between 30 and 100 $M_\odot$ are usually assumed in starburst models. It is, however, possible to constrain this parameter using the He I λ2.06 μm/Brγ ratio. Since the ionization potential of helium is twice that of hydrogen, the He I λ2.06 μm/Brγ ratio provides some information about the slope of the ultraviolet spectrum, more specifically about the relative number of massive stars. This technique has been fully described in Doyon et al. (1992). It was shown there that the He I λ2.06 μm/Brγ ratio has a strong dependence on spectral type, a dependence which also translates to the upper mass limit. Based on Figure 7 of Doyon et al., the ratio of 0.35 ± 0.04 observed on the nucleus of NGC 3256 (see Table 3) implies an upper mass limit of $\sim 30\ M_\odot$.

It is difficult to constrain the IMF index without making some assumption about the age of the burst. Although we could use the age estimate derived in the previous section, the inferred age may depend on the IMF parameters. Therefore, to avoid this potential problem we choose to constrain both the age and the IMF index at the same time using the following χ^2 analysis. Using the population synthesis model described earlier, a set of five observables (CO_{sp}, $\log |W_{Br\gamma}|$, $\log N_{Lyc}/L_{IR}$, the He I λ2.06 μm/Brγ ratio, and the absolute K-magnitude M_K) are calculated for several combinations of α and age, assuming $m_l = 0.1\ M_\odot$ and $m_u = 30\ M_\odot$ and a given time dependence for the SFR. For a given set of observables x_i, each with an uncertainty σ_i, and X_i, the corresponding quantity predicted by the model, the goodness of a given solution may be defined by the following χ^2 expression:

$$\chi^2(t_0, \alpha, M_*) = \sum_i \left[\frac{x_i - X_i(t_0, \alpha, M_*)}{\sigma_i} \right]^2 , \qquad (2)$$

where t_0 is the age of the burst, α is the IMF index, and M_* is the total mass participating in the burst. Good models are characterized by small values of χ^2. Given an estimate of M_*, a χ^2 is calculated for each pair (α, t_0). In principle, if there is a unique solution to the problem, one should find a minimum χ^2 in the plane (α, t_0).

The dynamical mass in NGC 3256 can be determined from the rotation curve of Feast & Robertson (1978). Within the central 3".5 of the optical nucleus, we derive a mass of 1.3×10^8 $M_\odot$, assuming a distance of 37 Mpc. This value should be regarded as highly uncertain since there is evidence that the dynamical center of this galaxy is offset from the optical and 2.2 μm nucleus by $\sim 5''$ to the west (Feast & Robertson 1978). One can also estimate the mass participating in the starburst from the amount of molecular gas in the nucleus. Using the CO map of Sargent et al. (1989) and assuming that the molecular gas is distributed as an exponential disk, we derive a total H_2 mass of 1.8×10^8 $M_\odot$ within the central 3".5. The fact that the two estimates are of the same order of magnitude shows that the relative fraction of molecular gas mass with respect to the total mass is very high, if not dominant. This is hardly surprising since the total molecular gas content of NGC 3256 is an order of magnitude higher than that in our Galaxy (Sargent et al. 1989). Since the mass estimates above seem to suggest a large fraction of molecular gas, we shall assume that the total mass is dominated by the gas; this is obviously uncertain, but this approach is very conservative for our analysis. Using the average of the two estimates above yields a mass of 1.6×10^8 $M_\odot$ which is *available* for forming stars. Of course, the mass participating in the burst is necessarily smaller since the star formation efficiency (SFE), that is, the efficiency by which the gas is converted into stars, is smaller than 100%. For instance, the SFE in our Galaxy is about 5% (Mezger 1978), but it could be as high as 50% in the nearby starburst M82 (Rieke et al. 1980). If we make the assumption that M82 and NGC 3256 have a similar SFE of about 50%, then 8×10^7 $M_\odot$ is a probable estimate of the mass participating in the burst. We shall adopt this value for the following analysis, bearing in mind that this estimate is very uncertain, perhaps by as much as a factor of 2. The implications of this uncertainty will be discussed later. The values of the other four observables used in the model are given in Table 3.

Figures 5*a*, 5*b*, and 5*c* show contour maps of the reciprocal χ^2 ($1/\chi^2$), calculated for different SFR history. These figures show that, for an exponential or delayed SFR, *the age and the IMF index are uniquely defined in the plane* (α, t_0). One can get a rough estimate of the uncertainty in α and t_0 by looking at the extent of the contours in Figure 5. These were drawn on a logarithmic scale, each one separated by "one sigma," that is, by a factor of $e^{1/2}$. The extent of the highest contour yields a 1 σ uncertainty (excluding the constant SFR diagram) of ~ 0.1 for the IMF index and 1–5 Myr for the age, depending on the time dependence of the SFR. As shown by the very extended contours of Figure 5*a*, a constant SFR yields relatively large uncertainties for t_0 and the IMF index compared with the other two cases. This "poor" solution does not necessarily imply that a constant SFR is poor representation of the star formation history in NGC 3256. The extent of the contours depends somewhat on the mass estimate adopted in the analysis. In other words, it is impossible, based on the χ^2 diagrams, to exclude any of the three SFR functions adopted as a good representation of the SFR history in NGC 3256.

To complement the χ^2 diagrams, a model summary is given in Table 4. The predictions of the "best" models, inferred from the analysis above, are given in the third line of each SFR history. For comparison, models calculated with a Salpeter and Scalo IMF are also presented (the same age inferred from the "best" model was assumed). For the three SFR functions investigated, the minimum χ^2 was found with an IMF index between 1.6 and 1.9 which is significantly flatter than either the solar neighborhood IMF derived by Scalo (1986; $\alpha = 2.85$) or Salpeter (1955; $\alpha = 2.35$). As seen in Table 4, models with a Scalo or Salpeter IMF can only reproduce 10%–30% of the observed ionization rate and 2.2 luminosity. It is interesting to note that a unique solution is also obtained with an exponential SFR even when the mass is excluded from the analysis. Indeed, if we omit M_K in the χ^2 expression, both the age and the IMF index remain uniquely defined. This point is illustrated in Figure 5*d* which shows a reciprocaal χ^2 diagram calculated for an exponentially decreasing SFR in which the constraint from the mass has been relaxed. This diagram yields an age of 12 Myr as previously inferred but a very uncertain IMF index, ranging from 1.3 to 2.9.

The mass participating in the burst is obviously a crucial parameter for constraining the IMF index. We can estimate an upper limit for the IMF index by conservatively assuming an SFE of 100%. This would increase the mass participating in

© American Astronomical Society • Provided by the NASA Astrophysics Data System

1994ApJ...421..101D

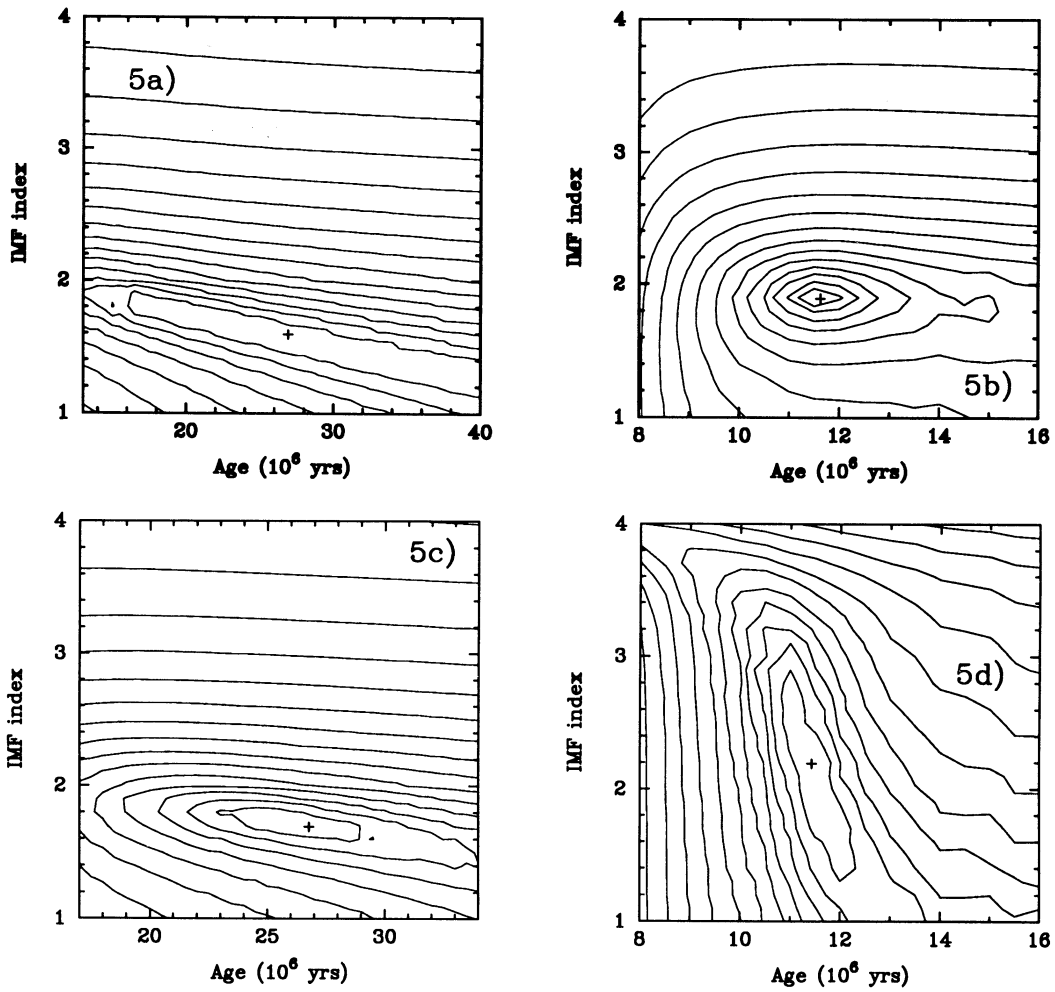

FIG. 5.—Reciprocal χ^2 diagram in the (α-age) plane for three different star formation rate histories: (*a*) constant, (*b*) exponential with a timescale of 20×10^6 yr, (*c*) "delayed" with the same timescale as in (*b*). The contours are drawn on a logarithmic scale, each one separated by "one sigma," i.e., by a factor of $e^{1/2}$. The highest contour is drawn 1 σ away from the peak. (*d*) Same as (*b*) except that the mass M_* participating in the burst has been excluded from the calculations (*see text*). The loci of the χ^2 minimum is indicated by a cross.

TABLE 4

MODEL SUMMARY FOR THE NUCLEUS OF NGC 3256[a]

Age (10^6 yr)	α[b]	M_K (mag)	CO_{sp}	log $W_{Br\gamma}$ (Å)	log N_{Lyc} (s^{-1})	log N_{Lyc}/L_{IR} (s^{-1} $L_\odot^{-1}$)	He I/Brγ	χ^2
			SFR = const					
27	Scalo	−19.89	0.29	1.20	52.74	42.99	0.35	811
27	Salpeter	−21.71	0.28	1.27	53.15	43.12	0.36	385
27	1.6	−22.55	0.27	1.38	53.99	43.25	0.38	5.2
			Exponential: $SFR \propto \exp(-t/\tau_0)$, $\tau_0 = 2 \times 10^7$ yr					
12	Scalo	−20.30	0.25	1.33	53.04	43.13	0.32	520
12	Salpeter	−21.23	0.25	1.36	53.45	43.21	0.34	181
12	1.90	−22.59	0.25	1.40	53.97	43.27	0.35	4.7
			Delayed: $SFR \propto t \exp(-t/\tau_0)$, $\tau_0 = 2 \times 10^7$ yr					
27	Scalo	−20.02	0.27	1.24	52.84	43.05	0.35	706
27	Salpeter	−20.87	0.28	1.31	53.25	43.16	0.36	307
27	1.70	−22.57	0.27	1.39	54.01	43.26	0.37	4.6
Target values		-22.55 ± 0.1	0.26 ± 0.01	1.40 ± 0.02	54.06 ± 0.04	43.12 ± 0.08	0.35 ± 0.04	

[a] All models are calculated with a mass M_* of 8×10^7 $M_\odot$.

[b] IMF index [$\psi(m) \propto m^{-\alpha}$] with $m_l = 0.1$ $M_\odot$ and $m_u = 30$ $M_\odot$. "Scalo" refers to the solar neighborhood IMF of Scalo 1986. The "Salpeter" IMF is equivalent to $\alpha = 2.35$.

© American Astronomical Society • Provided by the NASA Astrophysics Data System

1994ApJ...421..101D

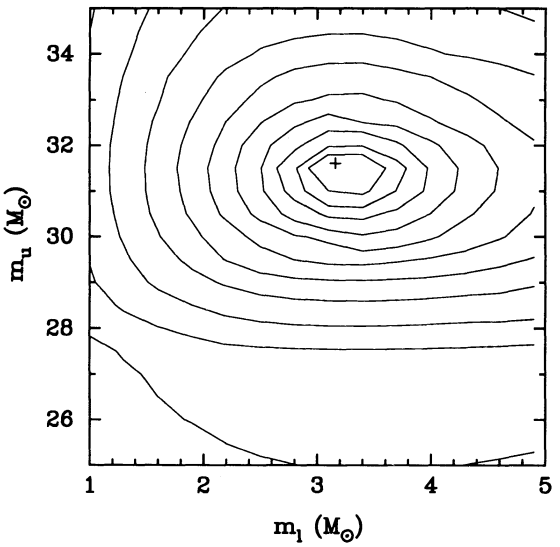

FIG. 6.—Reciprocal χ^2 diagram in the (m_u-m_l) plane, calculated using a Scalo IMF, an exponentially decreasing star formation rate, an age of 12×10^6 yr, and a mass M_* of $1.8 \times 10^8\ M_\odot$. The contours were drawn in the same way as described for Fig. 5.

the burst by a factor of 2, and the IMF index would become steeper going from 1.9 to 2.2 which is now marginally shallower than a Salpeter IMF.

The problem can also be parameterized in a different way, which consists of fixing both the IMF index and the age, and to determine the most likely combination of the mass limits, m_l and m_u, that satisfy the observations. This is, for instance, the strategy adopted by Rieke et al. (1980), Wright et al. (1988), and Puxley, Hawarden, & Mountain (1990). Using the same χ^2 analysis as described before, we calculated a χ^2 for several combinations of m_l and m_u, using a Scalo IMF, an exponentially decreasing SFR (arbitrarily chosen), an age of 12×10^6 yr (as suggested by Fig. 5*b*) and a mass of $8 \times 10^7\ M_\odot$. The resulting reciprocal χ^2 diagram is shown in Figure 6. Like Figure 5, there is a unique solution, this time at $m_l \sim 3\ M_\odot$ and $m_u \sim 31\ M_\odot$. Like the IMF index, the value of m_l or α depends somewhat on the adopted mass participating in the burst. Adopting a higher mass of $1.6 \times 10^8\ M_\odot$ (an SFE of 100%), the same analysis would yield $m_l = 1.6\ M_\odot$ and $m_u = 31\ M_\odot$. It is worthwhile to mention that the mass participating in the burst would have to increase by a factor of 7 (compared with the mass adopted for an SFE of 50%) for the model to reproduce the observations with a Scalo IMF and a lower mass limit of $0.1\ M_\odot$.

It thus seems that whatever approach we choose to constrain the stellar IMF parameters, it is difficult to avoid the conclusion that *the IMF in NGC 3256 is biased against the formation of low-mass stars.* Our analysis shows that the IMF in the nucleus of NGC 3256 is at least as flat as the Salpeter IMF which is among the shallowest IMFs inferred for the Galaxy and the Magellanic Clouds. Indeed, several IMF studies of OB associations in the Galaxy and the Magellanic Clouds (see Garmany 1992 for a review) yield IMF slopes ranging from 2.3 to 3.5. Further studies are definitely needed for determining whether this wide range of IMF slopes is real or due to systematics errors. Nevertheless, despite the uncertainties related with the universality of the IMF slope, the analysis above shows that it is possible to constrain objectively the IMF slope of distant stellar systems in which individual stars cannot be observed. As mentioned earlier, the mass participating in the burst is a very important observable in the analysis, and future observational efforts should concentrate in constraining this parameter with better accuracy. Determining the mass at high spatial resolution via velocity dispersion measurements in the IR (e.g., the CO bandhead at 2.3 μm) is now possible with the recent development of very sensitive IR long-slit spectrometers. Measuring the mass on circumnuclear starburst regions would be particularly valuable since the contamination problem by the old preexisting stellar population would be minimized.

5. SUMMARY AND CONCLUSIONS

We have presented NIR spectra of the nuclear region of the merging system NGC 3256. The spectra shows strong molecular hydrogen emission, recombination lines of hydrogen, helium, and [Fe II]. The relative strength of these lines and the strong CO band absorption are interpreted as evidence that NGC 3256 is experiencing an episode of vigorous star formation activity. Except for a 10% contribution of nonstellar free-free and hot dust emission, the 2.2 μm continuum of NGC 3256 is dominated by emission from red supergiants, the old preexisting stellar population contributing less than 25% of the total K continuum.

We have used a stellar population synthesis model to determine the age of the burst and the parameters of the IMF. The results of this modeling shows that the Brγ equivalent width and the strength of the CO band at 2.3 μm both provide a simple tool for constraining the age of the burst. With this technique, we derived an age of 12–27 Myr for the nucleus, depending on the detailed shape of the star formation rate. A χ^2 analysis technique was used to constrain both the age and the slope of the initial mass function in a unique way. Assuming that the IMF is extended down to $0.1\ M_\odot$ and up to $30\ M_\odot$, the observational properties of the galaxy are best fitted with an IMF index between 1.6 and 2.2, depending on the mass participating in the burst. This IMF slope is shallower than that recently inferred for the IMF in the solar neighborhood and the Magellanic Clouds and suggests that low-mass stars are relatively deficient in NGC 3256.

It is a pleasure to thank David Allen, Peter Meikle, and Jason Spyromilio for their help in using FIGS on the AAT. We are very grateful to Phil Puxley for many illuminating discussions. We are grateful to the referee for useful comments. R. D. is financially supported by a postdoctoral NSERC fellowship.

© American Astronomical Society • Provided by the NASA Astrophysics Data System

1994ApJ...421..101D

APPENDIX A

DEFINITION OF THE SPECTROSCOPIC CO INDEX

In their pioneering study of early-type galaxies, Frogel et al. (1978) established a photometric system for measuring the strength of the CO band based on two narrow-band ($\Delta\lambda = 0.08$ μm) filters centered on the CO dip at 2.36 μm and the nearby continuum at 2.2 μm. They defined a photometric "CO index" as the difference in magnitudes of the two filters relative to the difference for αLyrae, an A0V star which has no trace of CO absorption in its spectrum. The CO index is defined such that high values correspond to strong CO bands. Frogel et al. showed that the spectroscopic dependence of the CO absorption feature on temperature and luminosity is well represented by the CO index.

Although the CO index has been—and still is—a very important tool for studying the stellar content of early-type galaxies, it has some drawbacks. First, since the CO index is sensitive to the slope of the spectrum between 2.2 and 2.36 μm, this technique has serious limitations for measuring the depth of the CO band in such diverse systems as active galactic nuclei (AGNs) and starburst galaxies, where the slope of the K continuum is very often affected by high extinction and contaminated by nonstellar sources such as hot dust (600–1000 K) and nonthermal emission. Extinction and contamination from nonstellar sources make the spectrum redder than normal and thus artificially *decreases* the CO index. This effect has been shown to be very important in starburst galaxies (Doyon, Joseph, & Wright 1989, 1991).

Second, because the CO and continuum filters have a fixed wavelength, the CO index is redshift-dependent. Above a redshift of 3000 km s^{-1}, the K-correction on the CO index becomes unreliably large (see Arnaud & Gilmore 1986). Finally, the continuum filter used to define the CO index can be contaminated by Brγ emission. This contamination is small (<0.02 mag) in starbursts and AGNs where the K continuum is relatively strong but potentially important in weak continuum systems such as blue compact galaxies.

All of these problems can be avoided by measuring the strength of the CO band spectroscopically. We propose the following definition:

$$CO_{sp} \equiv -2.5 \log \langle R_{2.36} \rangle \tag{A.1}$$

where $\langle R_{2.36} \rangle$ is the average of the rectified spectrum between 2.31 and 2.40 μm in the rest frame of the galaxy. This definition was specifically chosen to be similar to the photometric CO index in order to allow a meaningful comparison between the two indices. Like the photometric CO index, CO_{sp} is defined such that the index is larger for deeper CO features. The rectified spectrum is obtained by fitting a power law ($F_\lambda \propto \lambda^\beta$) to featureless sections of the continuum between 2.0 and 2.29 μm. Given the approximate Rayleigh-Jeans nature ($F_\lambda \propto \lambda^{-4}$) of stellar spectra in the IR, the choice of a power law for fitting the continuum is physically justified.

Spectroscopic CO indices have been calculated for all 26 stars in the Kleinmann & Hall (1986) atlas. The spectra given in this atlas are ratioed with αLyrae or other A0 stars. In order to uncover the original energy distribution of the stars, the spectra were multiplied by a power-law continuum in the form $F_\lambda \propto \lambda^{-3.94}$ which is the closest representation of an A0 star (Kurucz 1979; as quoted by McGregor 1987). The resulting spectrum was then fitted with a power-law continuum which was used to rectify the spectrum and calculate the spectroscopic CO index using equation (A.1). Spectroscopic CO indices and fitted power-law indices are given in Table 5.

The dependence of the spectroscopic CO index on effective temperature is shown in Figure 7. Average temperatures were estimated from spectral types using the calibration given in Landolt-Börnstein (1982). The well-known strengthening of CO absorption with decreasing temperature and increasing luminosity is clearly reproduced in this figure. Within an accuracy of 0.015

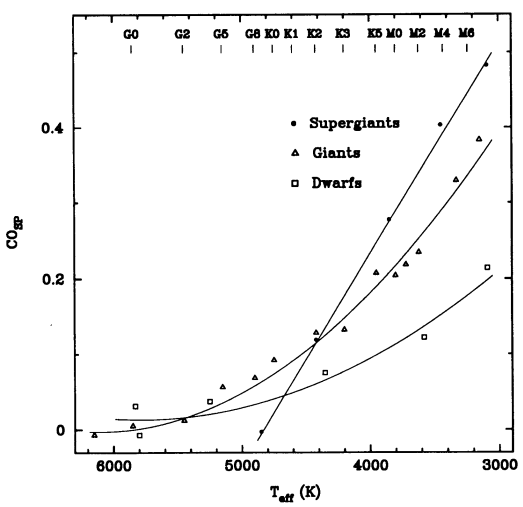

FIG. 7.—Dependence of the spectroscopic CO index on effective temperature and luminosity. The spectral type sequence of giant stars is indicated at the top of the figure. Solid lines are graphical representations of eqs. (A.2).

© American Astronomical Society • Provided by the NASA Astrophysics Data System

1994ApJ...421..101D

TABLE 5

SPECTROSCOPIC CO INDEX OF LATE-TYPE STARS

Name	Spectral Type	T_{eff} (K)	β[a]	CO_{ph}[b]	CO_{sp}
HR 8752	G5 0-Ia	4850	−3.3	...	−0.01
RW Cep	K0 0-Ia	4420	−3.1	...	0.11
BS 8726	K5 Ib	3850	−3.4	...	0.27
μ Cep	M2 Ia	3450	−2.8	...	0.40
SU Per	M3-M4 Iab	3090	−2.9	...	0.48
ν Peg	F8 III	6150	−3.9	...	−0.01
31 Com	G0 IIIp	5850	−3.9	...	0.00
84 Her	G2 IIIb	5450	−3.9	...	0.01
o UMa	G5 IIIa	5150	−3.6	0.03	0.05
ϵ Vir	G8 IIIab	4900	−3.7	0.04	0.06
ι Cep	K0- III	4750	−3.9	0.07	0.09
κ Oph	K2 III	4420	−3.7	0.11	0.12
39 Cyg	K3 III	4200	−3.8	0.12	0.13
γ Dra	K5 III	3950	−3.6	0.15	0.20
γ Sge	M0- III	3800	−3.7	0.17	0.20
χ Peg	M1 III	3720	−3.6	0.18	0.21
R Lyr	M5 III	3330	−3.3	0.23	0.32
BK Vir	M7-III	3150	−3.0	0.25	0.38
SW Vir	M7 III:	3150	−2.9	0.25	0.36
16 Cyg A	G3 V	5830	−3.7	...	0.03
16 Cyg B	G4 V	5800	−4.3	...	−0.01
σ Dra	K0 V	5250	−3.6	0.02	0.03
61 Cyg A	K5 V	4350	−3.7	0.04	0.07
Gl 411	M2+ V	3580	−2.1	0.03	0.12
Wolf 359	M5.8 V	3090	−1.3	−0.03	0.21

[a] Index of the power-law continuum ($F_\lambda \propto \lambda^\beta$) fitted to the spectrum shortward of 2.29 μm.

[b] Average photometric CO index for the corresponding spectral type. From Frogel et al. 1978.

mag, the following analytical expressions may be used to derive the spectroscopic CO index from the effective temperature:

$$\begin{aligned} \text{Dwarfs: } CO_{sp} &= 0.866 - 2.95T_4 + 2.55T_4^2 , \\ \text{Giants: } CO_{sp} &= 1.530 - 5.01T_4 + 4.10T_4^2 , \\ \text{Supergiants: } CO_{sp} &= 1.353 - 2.80T_4 , \end{aligned} \tag{A.2}$$

where T_4 is the effective temperature in units of 10^4 K. These expressions are valid at any temperature as long as CO_{sp} is positive. The spectroscopic CO index should be set to zero when the expressions above yield a negative value.

Average photometric CO indices taken from Frogel et al. (1978) are also given in Table 5. These indices are averages based on several measurements of different stars of the same spectral type. The true CO index of the stars listed in Table 5 is not necessarily the same as these averages but should not differ by more than 0.02 mag.

As expected, we found a very good correlation between the photometric and spectroscopic CO indices of giants and supergiants. Dwarfs were excluded from this comparison because the water absorption at 2 μm is strong enough to contaminate the continuum filter significantly. As a result, the photometric CO index of dwarfs is not very representative of the true CO absorption in their spectrum. The following transformation may be used between the indices:

$$CO_{sp} = 1.46CO_{ph} - 0.02 , \tag{A.3}$$

where CO_{ph} is the photometric CO index. This transformation is also valid for any giant/supergiant dominated stellar system.

The accuracy of the spectroscopic CO index is limited by the uncertainty in fitting the power-law continuum. When the spectrum is not affected by strong water absorption at 2 μm, this uncertainty is essentially limited by the signal-to-noise of the data. In practice, the error on the power-law index has a negligible (<0.01 mag) effect on the spectroscopic CO index for S/N > 40.

If the spectrum is strongly affected by water absorption, a common feature in very late-type stars (later than $\sim$M5), the error on CO_{sp} is then dominated by the systematic uncertainty in fitting the power-law continuum, even if the signal-to-noise is very high. In practice, it was found that this systematic uncertainty never exceeds ~ 0.05 mag, which is relatively small given that the typical CO_{sp} is greater than ~ 0.3 for very late-type dwarfs (see Table 5).

APPENDIX B

DESCRIPTION OF THE STARBURST MODEL

The model used in this paper is similar to that used by Tinsley (1968, 1972), Huchra (1977), and Bruzual (1983). The technique consists of following the evolution of stars in the Hertzsprung-Russell (HR) diagram according to known evolutionary tracks, for a

© American Astronomical Society • Provided by the NASA Astrophysics Data System

1994ApJ...421..101D

given initial mass function and a star formation rate. The tracks provide the bolometric luminosity L and the effective temperature $T_{\rm eff}$ as a function of time. Let $N(m, t)$ be the number of stars with progenitor mass m at the evolutionary stage t. After a time t_0, the number of stars in the interval $[t, t + dt]$ is given by

$$dN(m, t, t_0) = R_N(t_0 - t)\psi(m)dm\,dt, \qquad t < t_0\ , \tag{B.1}$$

where $\psi(m)$ is the IMF, the number of stars formed per unit mass interval. R_N is the SFR in units of stars per year. The total mass, $dM(t, t_0)$, of all the stars at the evolutionary stage, $[t, t + dt]$, can be obtained by multiplying the right side of equation (B.1) by m and integrating over the mass, from m_l to m_u, the lower and upper mass limits of the IMF, respectively. Let $R_M(t)$ be the SFR in units of mass per year and defined as $dM(t)/dt$. It follows from equation (B1), that R_M and R_N are related by the following expression

$$R_M(t) = R_N(t)\int_{m_l}^{m_u}\psi(m)m\,dm\ . \tag{B.2}$$

The lifetime t_0 of the model under consideration is divided up into a large number n (usually 1000) of time steps of equal duration $\Delta\tau$ such that $t_0 = n\Delta\tau$. Let $f(m_i, t)$ be the flux[1] of a star with progenitor mass m_i at the evolutionary stage t. If there are a number l of evolutionary tracks available, then the total flux $F(t_0)$ contributed by stars of all types after a time t_0 is given by

$$F(t_0) = \frac{1}{\int_{m_l}^{m_u}\psi(m)m\,dm}\sum_{j=0}^{n-1}\sum_{i=1}^{l}\int_{m_1}^{m_2}\psi(m)dm\int_{(n-j-1)\Delta\tau}^{(n-j)\Delta\tau}R_M(t_0 - t)f(m_i, t)dt \tag{B.3}$$

with $m_1 = (m_{l-1}\,m_l)^{1/2}$ and $m_2 = (m_l\,m_{l+1})^{1/2}$, as in Tinsley (1972). The normalization of equation (B.3) is such that

$$\int_{m_l}^{m_u}\psi(m)dm = 1$$

and

$$\int_0^{t_0}R_M(t)dt = M_0\ , \tag{B.4}$$

where M_0 is the total mass of stars ever formed since the beginning of the burst. The IMF is assumed to follow a power law of the mass with index $\alpha[\psi(m) \propto m^{-\alpha}]$. The evolutionary tracks used in the model were taken from Maeder & Meynet (1988). These models include 21 masses ranging from 0.85 to 120 $M_\odot$, calculated for a solar metallicity ($Z = 0.02$). In order to increase the mass resolution, additional models were interpolated from the original 21 tracks. A set of 14 unevolved models (dwarf stars) with masses $<0.85\ M_\odot$ were also added to the evolutionary tracks in order to cover the lower main sequence. These models were assumed not to evolve on the timescale of a Hubble time.

Every point in the $\log L - \log T_{\rm eff}$ plane of the theoretical evolutionary tracks must be converted into age-flux tables. In practice, this procedure requires determining the spectral type and luminosity class of all the points in the HR diagram. For simplicity, it was assumed that all stars in the HR diagram can be described either as a dwarf (main-sequence star), giant, or supergiant star. Although a Wolf-Rayet (W-R) stage is predicted by the theoretical evolutionary tracks for the most massive stars ($>30\ M_\odot$), the observational properties of W-R stars were not included in the model because of their relatively short lifetime ($\sim 10^5$ yr). Instead, their properties were approximated either as hot main-sequence or supergiant stars. The exclusion of W-R stars should have little effect on the prediction of broad-band colors and ionization rates provided that the model under consideration is older than ~ 5 Myr.

The calibration between effective temperature and spectral type and the conversion between bolometric luminosities and absolute V-magnitude were taken from the compilation of stellar properties of Landolt-Börnstein (1982).

The "flux" in a filter i, for a star of type k is defined as

$$F_i^k \equiv 10^{-M_i^k/2.5}\ , \tag{B.5}$$

where M_i^k is the absolute magnitude in the filter i of a star of type k.

NIR JHK and $V-K$ colors were taken from Frogel et al. (1978) for dwarfs and giants later than G5 and from Johnson (1966) for earlier stars. Johnson did not provide $VJHK$ colors for early-type giants. It was assumed that these stars have the same colors as early-type dwarfs. Comparison of their UBV colors shows that this is a very good approximation for stars earlier than F5. Colors of giants with spectral type between F5 and G5 were interpolated smoothly from those of Johnson and Frogel et al.. For consistency, the same interpolation procedure was applied to dwarfs with spectral type between F5 and G5.

Because Johnson's $J-K$ colors are systematically redder compared with Frogel's, the former were converted into the Frogel et al. (or CIT) system using a transformation derived from the colors of giants given in Frogel et al. (1978) and Johnson (1966):

$$(J-K)_{\rm Frogel} = 0.92(J-K)_{\rm Johnson} + 0.001\ . \tag{B.6}$$

Since $J-H$ colors are not available for stars earlier than G5, the latter were calculated by interpolating from Johnson's IJK colors assuming a power law for the stellar energy distribution between I and K. $VJHK$ colors of supergiants later than K3 were taken from Elias, Frogel, & Humphreys (1985). Other spectral types were interpolated from Johnson's IJK colors as described above.

Spectroscopic CO indices were calculated from the effective temperature using the analytical expressions given in Appendix A.

[1] The use of the term "flux" is very general and refers to any physical quantity associated with a star (e.g., bolometric luminosity, band flux, ionization rate, etc.).

© American Astronomical Society • Provided by the NASA Astrophysics Data System

1994ApJ...421..101D

The flux in the CO filter of a star of type k is defined as

$$F^k_{\rm CO} \equiv F^k_K 10^{-CO_{\rm sp}{}^k/2.5}\,, \tag{B.7}$$

where $CO^k_{\rm sp}$ is the spectroscopic CO index and F^k_K the flux in the 2.2 μm filter.

Ionization rates for photons with energy greater than 13.6 eV (the ionization potential of hydrogen), $N^{\rm H}_{\rm Lyc}(T_{\rm eff})$, were taken from Puxley (1988; see also Puxley et al. 1990) for main-sequence stars. Those were calculated by integrating under Kurucz (1979) atmosphere models.

For consistency, the ionization rates of giants and supergiants were calculated in a similar way from Kurucz's models using a program kindly provided by Phil Puxley. Adopted stellar properties (mass, radius, and surface gravity) were taken from Landolt-Börnstein (1982). Because giant and supergiant models with effective temperatures $>30{,}000$ K are not available from Kurucz, the ionization rates of these stars were estimated from those of main-sequence stars of the same temperature assuming the ionization rate ratios (giants/dwarf, supergiant/dwarf) derived from the data of Panagia (1973). In order to calculate the strength of helium recombination lines, a second ionization rate, $N^{\rm He}_{\rm Lyc}(T_{\rm eff})$, was also calculated in the same way by integrating Kurucz models beyond the ionization potential of helium (24.6 eV).

REFERENCES

Allen, D. 1989, FIGS User's Manual (Anglo-Australian Observatory), 47
Arnaud, K. A., & Gilmore, G. 1986, MNRAS, 220, 759
Bailey, J., et al. 1988, PASP, 100, 1178
Bruzual, G. A. 1983, ApJ, 273, 105
Devereux, N. A., Becklin, E. E., & Scoville, N. Z. 1987, ApJ, 312, 529
Doyon, R., Joseph, R. D., & Wright, G. S. 1989, in 22d Eslab Symp., Infrared Spectroscopy in Astronomy, ed. B. H. Kaldeich, 477
———. 1991, in Astrophysics with Infrared Arrays, ed. R. Elston (ASP Conf. Ser. 14), 69
Doyon, R., Puxley, P. J., & Joseph, R. D. 1992, ApJ, 397, 117
Doyon, R., Wright, G. S., & Joseph, R. D. 1994, ApJ, 421, 115
Draine, B. T. 1989, in 22d Eslab Symp., Infrared Spectroscopy in Astronomy, ed. B. H. Kaldeich, 93
Elias, J. A., Frogel, J. A., & Humphreys, R. M. 1985, ApJS, 57, 91
Feast, M. W., & Robertson, B. S. C. 1978, MNRAS, 185, 31
Frogel, J. A. 1985, ApJ, 298, 528
Frogel, J. A., Cohen, J. G., & Persson, S. E. 1983, ApJ, 275, 773
Frogel, J. A., Persson, S. E., Aaronson, M., & Matthews, K. 1978, ApJ, 220, 75
Garmany, C. D. 1992, in Massive Stars in Starbursts, ed. C. Leitherer, N. R. Walborn, T. M. Heckman, & C. A. Norman, 115
Graham, J. R., Wright, G. S., Joseph, R. D., Frogel, J. A., Phillips, M. M., & Meikle, W. P. S. 1987, in Star Formation in Galaxies, ed. C. J. Persson (Washington: GPO), 517
Graham, J. R., Wright, G. S., & Longmore, A. J. 1987, ApJ, 313, 847
Graham, J. R., Wright, G. S., Meikle, W. P. S., Joseph, R. D., & Bode, M. F. 1984, Nature, 310, 2313
Huchra, J. P. 1977, ApJ, 217, 928
Hummer, D. G., & Storey, P. J. 1987, MNRAS, 224, 801
Humphreys, R. 1978, ApJS, 38, 309
Johnson, H. L. 1966, ARA&A, 4, 193
Joseph, R. D., & Wright, G. S. 1985, MNRAS, 214, 87
———. 1994, in preparation
Joseph, R. D., Wright, G. S., Wade, R., Graham, J. R., Gatley, I., & Prestwich, A. H. 1987, in Star Formation in Galaxies, ed. C. J. Persson (Washington: GPO), 421
Joy, M., & Lester, D. F. 1988, ApJ, 331, 145
Kleinmann, S. G., & Hall, D. N. B. 1986, ApJS, 62, 501
Kurucz, R. L. 1979, ApJS, 40, 1
Landolt-Börnstein. 1982, Star and Star Clusters, ed. K. Schiaffers & H. H. Voigt, A&A, 26
Lester, D. F., Carr, J. S., Joy, M., & Gaffney, N. 1990, ApJ, 352, 544
Maeder, A., & Meynet, G. 1988, A&AS, 76, 411
McGregor, P. J. 1987, ApJ, 312, 195
Mezger, P. G. 1978, in Infrared Astronomy, ed. G. Setti & G. Fazio (Dordrecht: Reidel), 1
Miller, G. E., & Scalo, J. M. 1979, ApJS, 41, 513
Moorwood, A. F. M., & Oliva, E. 1988, A&A, 203, 278
Nussbaumer, H., & Storey, P. J. 1988, A&A, 193, 327
Panagia, N. 1973, AJ, 78, 9
Prestwich, A. H. 1989, Ph.D. thesis, Imperial College, Univ. London
Puxley, P. J. 1988, Ph.D. thesis, Univ. Edinburgh
Puxley, P. J., Brand, P. W. J. L., Moore, T. J. T., Mountain, C. M., Nakai, N., & Yamashita, T. 1989, ApJ, 345, 163
Puxley, P. J., Hawarden, T. G., & Mountain, C. M. 1990, ApJ, 364, 77
Rieke, G. H., Lebofsky, M. J., Thompson, R. I., Low, F. J., & Tokunaga, A. T. 1980, ApJ, 238, 24
Salpeter, E. 1955, ApJ, 121, 161
Sargent, A. I., Sanders, D. B., & Phillips, T. G. 1989, ApJ, 346, L9
Scalo, J. M. 1986, Fund. Cosmic Phys., 11, 1
———. 1989, in Windows on Galaxies, ed. A. Renzini, G. Fabianno, & J. S. Gallagher (Dordrecht: Kluwer), 125
Schweizer, F. 1986, Science, 231, 227
Scoville, N. Z., Becklin, E. E., Young, J. S., & Capps, R. W. 1983, ApJ, 271, 512
Telesco, C. M., & Gatley, I. 1984, ApJ, 284, 557
Tinsley, B. 1968, ApJ, 151, 547
———. 1972, A&A, 20, 383
Toomre, A., & Toomre, J. 1972, ApJ, 178, 623
Wright, G. S., Joseph, R. D., Robertson, N. A., James, P. A., & Meikle, W. P. S. 1988, MNRAS, 233, 1

© American Astronomical Society • Provided by the NASA Astrophysics Data System